

SLAC-PUB-6314
August, 1993
(T/E)

Photon-Photon Collisions at the Next Linear Collider: Theory^{*}

STANLEY J. BRODSKY

*Stanford Linear Accelerator Center
Stanford University, Stanford, California 94309*

ABSTRACT

The collisions of photons at a high energy electron-positron collider provide a comprehensive laboratory for testing QCD, electroweak interactions, and extensions of the standard model. It is expected that by using back-scattered laser beams, that the effective luminosity and energy of photon-photon collisions will be comparable to that of the primary e^+e^- collisions. In this talk, I will focus on tests of electroweak theory in photon-photon annihilation such as $\gamma\gamma \rightarrow W^+W^-$, $\gamma\gamma \rightarrow$ Higgs bosons, and higher-order loop processes, such as $\gamma\gamma \rightarrow \gamma\gamma, Z\gamma$ and ZZ . Since each photon can be resolved into a W^+W^- pair, high energy photon-photon collisions can also provide a remarkably background-free laboratory for studying WW collisions and annihilation. I also review high energy $\gamma\gamma$ tests of quantum chromodynamics, such as the scaling of the photon structure function, $t\bar{t}$ production, mini-jet processes, and diffractive reactions.

Presented at the Second International Workshop on
Physics and Experiments with Linear Colliders
Waikoloa, Hawaii, April 26-30, 1993

^{*} Work supported by the Department of Energy, contract DE-AC03-76SF00515.

Photon-Photon Collisions at the Next Linear Collider: Theory

STANLEY J. BRODSKY

*Stanford Linear Accelerator Center
Stanford University, Stanford, California 94309*

ABSTRACT

The collisions of photons at a high energy electron-positron collider provide a comprehensive laboratory for testing QCD, electroweak interactions, and extensions of the standard model. It is expected that by using back-scattered laser beams, that the effective luminosity and energy of photon-photon collisions will be comparable to that of the primary e^+e^- collisions. In this talk, I will focus on tests of electroweak theory in photon-photon annihilation such as $\gamma\gamma \rightarrow W^+W^-$, $\gamma\gamma \rightarrow$ Higgs bosons, and higher-order loop processes, such as $\gamma\gamma \rightarrow \gamma\gamma$, $Z\gamma$ and ZZ . Since each photon can be resolved into a W^+W^- pair, high energy photon-photon collisions can also provide a remarkably background-free laboratory for studying WW collisions and annihilation. I also review high energy $\gamma\gamma$ tests of quantum chromodynamics, such as the scaling of the photon structure function, $t\bar{t}$ production, mini-jet processes, and diffractive reactions.

1. Introduction

One of the most important areas of investigation at the next electron-positron linear collider will be the study of photon-photon collisions.^{1,2,3,4,5,6} Since photons couple directly to all fundamental fields carrying the electromagnetic current—leptons, quarks, W 's, supersymmetric particles, etc.—high energy $\gamma\gamma$ collisions can provide a laboratory for exploring virtually every aspect of the Standard Model and its extensions. For example, the incident photons can directly annihilate into W pairs or $q\bar{q}$ pairs at the tree graph level, or pairs of gluons, Z^0 's, or one or more Higgs bosons through quark and W box graphs. Two real photons can couple to any even charge conjugation resonance, unless it has spin $J = 1$, in which case it can be identified via its virtual photon couplings. In $\gamma\gamma$ events where each incident photon produces a W -pair, the e^+e^- collider becomes the equivalent of a tagged WW collider, allowing the study of WW scattering and annihilation and a new domain of electroweak and Higgs physics.⁷

Because of the simplicity of its initial state, two-photon collisions provide an

important laboratory for testing coherent and incoherent effects in quantum chromodynamics. In QCD events where each photon is resolved⁸ in terms of its intermediate quark and gluon states, $\gamma\gamma$ collisions resemble point-like meson-meson collisions. In the case of exclusive final states such as $\gamma\gamma \rightarrow p\bar{p}$ or meson pairs, two photon collisions provide a time-like Compton microscope for measuring distribution amplitudes, the fundamental wavefunction of hadrons.^{9,10} One can study detailed features of $\gamma\gamma \rightarrow t\bar{t}$ at threshold and its final state evolution. In the case of single or double diffractive two-photon events, one can study fundamental aspects of pomeron and odderon t -channel physics.¹¹ One can also utilize electron-photon collisions at a linear collider and test other fundamental aspects of QCD such as the shape and growth of the photon structure function and the structure of photon to meson transition form factors.¹²

All of the physics programs which I will discuss in this report appear to be experimentally feasible at an NLC, since by using back-scattered laser beams, it is expected that the $\gamma\gamma$ luminosity will be comparable to the electron-positron luminosity, and that high photon energy fractions and polarization can be attained.¹³

2. Sources of $\gamma\gamma$ Collisions

In an e^+e^- or e^-e^- linear collider there are three main sources of photon-photon collisions. The first is the equivalent photon spectrum in which the virtual bremsstrahlung has the relatively soft spectrum $G_{\gamma/e}(x, Q^2) \sim \frac{\alpha}{2\pi} \log \frac{s}{M_e^2} \frac{1+(1-x)^2}{x}$. The equivalent photon approximation applied to each of the incident leptons gives cross sections analogous to the QCD factorization formula for fusion processes in high transverse momentum inclusive reactions.¹⁴ Virtual bremsstrahlung has been the traditional mode for studying two-photon physics at e^+e^- storage rings, and it will continue to be very important at the next generation of B-factories. By tagging the scattered electron one can also select photons with a given spacelike mass and polarization. Thus, in the case of tagged electron-electron or electron-photon collisions, the photon mass itself becomes a variable.

Equivalent beams of real photons are also created in high luminosity linear colliders by the "beamstrahlung" process in which an electron going through the opposing high density bunch of positrons scatters and radiates a spectrum of nearly collinear photons.^{15,16} The beamstrahlung photons are unpolarized, but the spectrum can be considerably harder than that of the corresponding equivalent photon spectrum.¹⁷

It appears that the most advantageous way to initiate photon-photon collisions at the next linear collider will be to use a back-scattered laser beam, as pioneered by Ginzburg *et al.*¹³ In this process, photons from a laser beam of eV energies

are scattered against an electron or positron beam to produce a nearly collinear beam of high energy photons. Ideally, the polarized laser beam back-scatters on a polarized electron beam thus converting each electron into a photon with a high fraction of its energy. Unlike the beamstrahlung and equivalent photon processes, the effective e^+e^- and laser-induced high energy $\gamma\gamma$ luminosities can be comparable. The extraordinary energy and high luminosity of the back-scattered laser collisions promise to make two-photon physics a key component of the physics program of the next linear collider.

In principle, each of the three types of photon beams can collide with each other, so there are actually nine possible $\gamma\gamma$ collisions at a linear collider; one also has the possibility of real photons colliding with tagged virtual photons through photon-electron collisions.¹⁸

3. Survey of Photon-Photon Collider Processes

Figure 1 illustrates many of the $\gamma\gamma$ processes which could be studied at an NLC.

1. The simplest reactions are the direct $\gamma\gamma$ couplings to pairs of leptons, W 's, and quarks. Any energetically accessible particle which carries the electromagnetic charge, including supersymmetric and technicolor particles, can be produced in pairs. In each case, the charged line can then radiate its respective gauge partners: *e.g.*, photons, gluons, Z 's as well as Higgs bosons.
2. As shown in Figure 1b, one can produce pairs of charge-less fundamental particles in $\gamma\gamma$ collisions through quantum loop diagrams, as in the traditional light-by-light scattering box graph. For example, two photons can annihilate and produce two outgoing photons or a pair of co-planar Z 's through virtual W and quark loops. A pair of gluon jets can be produced through a quark box diagram. A single Higgs boson or an excited Z' can be produced through triangle graphs.¹⁹
3. At high energies, one or both of the an incident photons can "resolve" itself as a pair of fundamental charged particles which can then interact via scattering subprocesses. Thus, as illustrated in Fig. 1c, a photon can develop into a Fock state of $q\bar{q}$ or W^+W^- or leptonic pairs, which then interact by $2 \rightarrow 2$ processes; *e.g.*, quark-quark scattering through gluon exchange or top-quark scattering through Higgs exchange. In addition, one can have interactions of a directly coupled photon with the resolved constituent of the other photon.

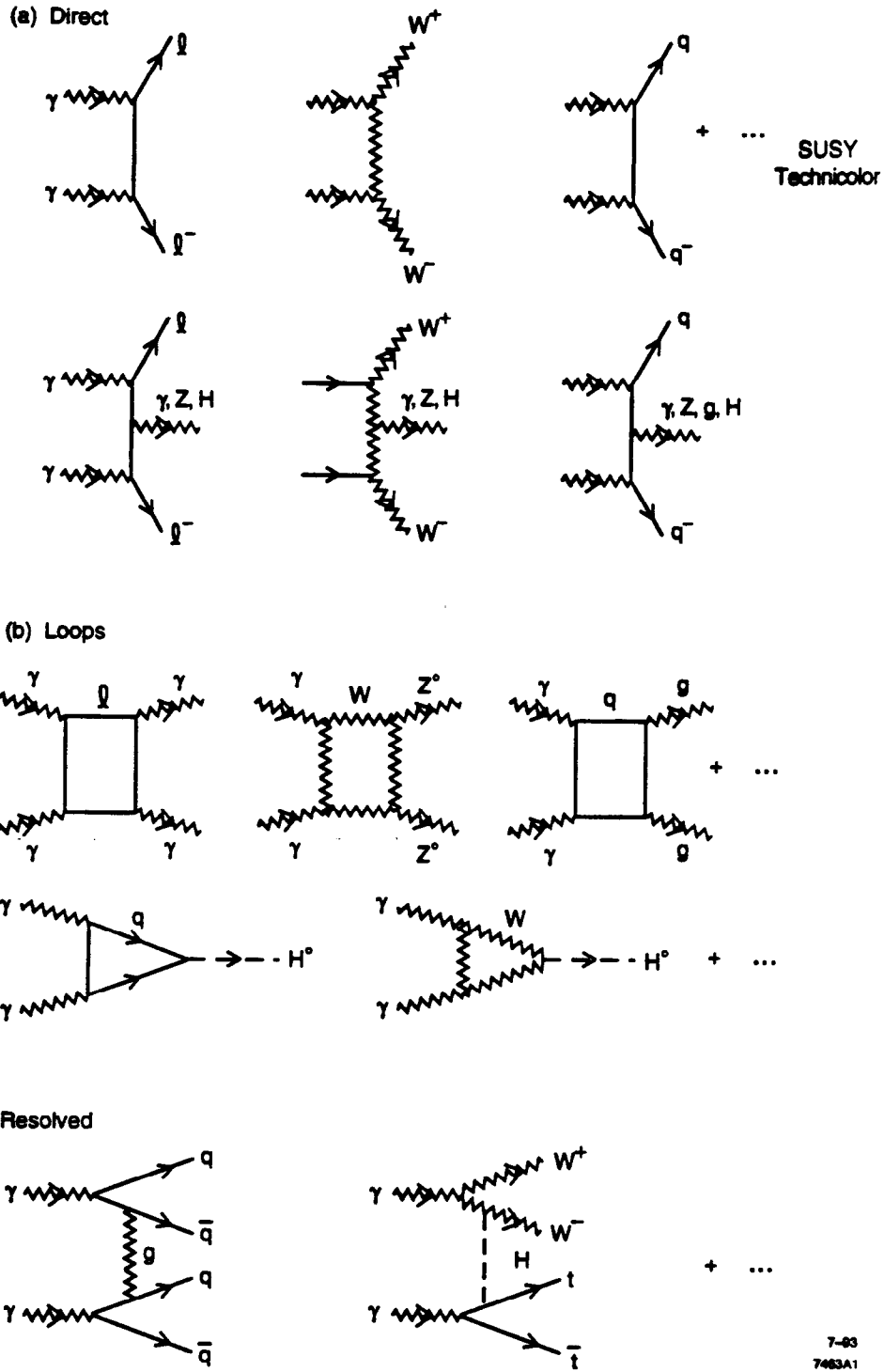


Figure 1. Illustration of direct, resolved, and higher-order loop contributions to high energy gg collisions.

4. The Photon's Light-Cone Fock Expansion

One can distinguish the various contributions to the photon's direct and resolved interactions in the following way: Consider the Lagrangian for the Standard Model cutoff at an ultraviolet scale Λ and the corresponding light-cone time $\tau = t - z/c$ evolution operator; *i.e.*, the light-cone Hamiltonian $H_{LC}^{(\Lambda)}$. The photon is the physical zero-mass eigenstate of the full Hamiltonian. Any eigenstate of the full Hamiltonian can be expanded as a sum of eigenstates of the free Hamiltonian: $|\psi\rangle = \sum_n |n\rangle \langle n|\psi\rangle$. The photon state is thus equivalent to a coherent sum of free Fock states with the same charge and color singlet quantum numbers. The coefficients in this expansion, $\langle n|\psi\rangle = \psi_{n/\gamma}^{(\Lambda)}(x_i, \vec{k}_{\perp i}, \lambda_i)$, with $\sum x_i = 1$ and $\sum \vec{k}_{\perp i} = 0$ are the basic wavefunction matrix elements needed to describe the photon in terms of its quark and gluon and other Standard Model degrees of freedom. The $\psi_{n/\gamma}^{(\Lambda)}(x_i, \vec{k}_{\perp i}, \lambda_i)$, are frame independent functions of the light-cone fractions $x_i = k_i^+/p^+$, the relative transverse momenta $k_{\perp i}$, and the spin projections λ_i .¹² Since the photon is an elementary field, the physical photon has a non-zero bare component in the Fock expansion: $\psi_{\gamma}^0(x, k_{\perp}) = 16\pi^3 \sqrt{Z_3(\Lambda^2)} \delta(1-x) \delta^2(\vec{k}_{\perp}) \delta_{\lambda\lambda'}$, where $Z_3(\Lambda^2)$ is the probability that the photon stays a bare photon at the cutoff scale Λ .

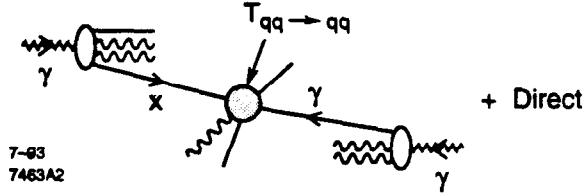


Figure 2. Factorization of the resolved photon-photon amplitudes using the light-cone Fock basis. In the case of the direct contributions, the photon annihilates within the hard scattering amplitude.

Given the photon's Fock expansion we can calculate the photon-photon scattering amplitude at high momentum transfer in terms of its constituents' interactions in the factorized form shown in Fig. 2 and

$$\mathcal{M} = \sum_{n,m} \int \frac{\pi d^2 k_{\perp} dx}{16\pi^3} \psi_n^{(\Lambda)}(x_i, k_{\perp i}, \lambda_i) \int \frac{\pi d^2 \ell_{\perp} dy}{16\pi^3} \psi_m^{(\Lambda)}(y_i, \ell_{\perp i}, \lambda_i) T_{ab \rightarrow cd}^{(\Lambda)}.$$

Here $T_{ab \rightarrow cd}^{(\Lambda)}$ is a sum over all $2 \rightarrow 2$ processes. It is irreducible and contains all the interactions, radiative corrections, and loop corrections with k_{\perp}^2 greater than the separation scale Λ^2 . Higher particle processes are generally higher twist and thus power-law suppressed at large momentum transfer. In the expansion of the

$\gamma\gamma$ scattering amplitude one thus obtains the direct pair production processes from the bare photon components as well as the resolved contributions. One can then square the matrix element, integrate over undetected variables, and derive the usual factorized form for hard scattering processes in QCD, but with the special addition of contributions from the direct-direct and direct-resolved $\gamma\gamma$ processes.

5. Studying WW scattering at a Photon Linear Collider

One of the most interesting potential applications of photon-photon collisions at a high energy linear collider is WW scattering, as illustrated in Fig. 3.

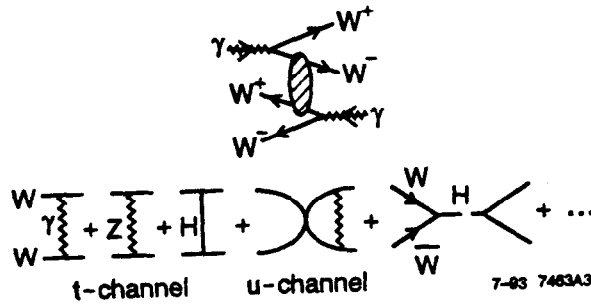


Figure 3. Illustration of WW scattering at a photon-photon collider. The kinematics of the interacting W 's can be determined by tagging the spectator W 's. The interacting pair can scatter or annihilate, for example into a Higgs boson.

In this process⁷ each photon is resolved as a WW pair. The interacting vector bosons can then scatter pair-wise or annihilate; *e.g.*, they can annihilate into a Standard Model Higgs boson²⁰ or a pair of top quarks. In principle, one can use this process as a nearly background-free laboratory for studying WW interactions. The scattering reaction leads to two W 's emerging at large transverse momentum in the final state accompanied by two W 's at $p_T \sim M_W$ focussed along the beam direction. We can estimate the cross section for $\gamma\gamma \rightarrow WWWW$ to be of order $\sigma_{\gamma\gamma \rightarrow WWWW} \sim \left(\frac{\alpha}{\pi}\right)^2 \log^2 \frac{s}{M_W^2} \sigma_{WW \rightarrow WW}$. Since the splitting function of photon into spin-one particles has a simple structure as a function of x , transverse momentum, and helicity, one has the potential to focus on specific W helicities and WW channels.

The splitting function for $\gamma \rightarrow W^+W^-$ can be relatively flat for some W helicities, so that one has a high probability for the W 's to scatter with a high fraction of the energy of the photon. One can thus study tree graphs contributions derived from photon, Z , or Higgs exchange in the t -channel, and $\Pi\Pi$ in the case of identical W 's, the additional u -channel amplitudes. In the case of oppositely-charged W 's, s -channel annihilation processes such as $W^+W^- \rightarrow t\bar{t}$ contribute. The largest cross sections

will arise if the W 's obey a strongly coupled theory; in this case the longitudinal W 's scattering amplitude saturates unitarity and the corresponding $\gamma\gamma \rightarrow WWWW$ cross section will be maximal.

6. Photon Structure Functions at the Next Linear Collider

A classical test of QCD in $\gamma\gamma$ collisions is the study of the photon structure functions,^{21,22} $F_i^\gamma(x, Q^2), i = 1, 2, 3$. (See Fig. 4.) At an NLC the back-scattered laser beam provides a high energy polarized target photon, and the neutral current probe is obtained by tagging the scattered electron at momentum transfer squared Q^2 . One can also reconstruct the charged current contributions where the electron scatters into a neutrino from calorimetric measurements of the recoiling system. It also should be possible to identify the separate charm, bottom, top and W contributions to the photon structure functions.

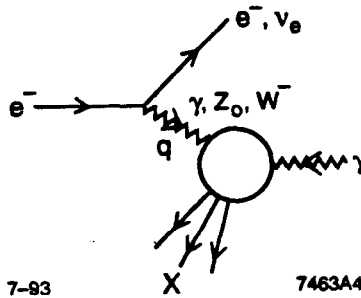


Figure 4. Neutral and charged current contributions to the photon structure function.

The photon structure function receives hadron-like contributions from the photon's resolved Fock components as well as its direct component derived from the $\gamma^*\gamma \rightarrow q\bar{q}$ timelike QCD Compton amplitude. Because of the direct contributions, the photon structure functions obey an inhomogeneous evolution equation:²³ The result, as first shown by Witten,²⁴ is that the leading order QCD structure functions of the photon have a unique scaling behavior: $F_1(x, Q^2) = h(x) \ln \frac{Q^2}{\Lambda^2}$, $F_2(x, Q^2) = f_2(x)$, $F_3(x, Q^2) = f_3^{\text{Box}}(x)$. Higher order contributions have been computed by a number of authors. In particular, the effects of heavy quarks at leading and next-to-leading order in α_s have been computed in detail by E. Laenen, *et al.*²⁵ A comparison of the QCD predictions given by Laenen *et al.* with data from the PLUTO experiment at PETRA for the photon structure function at $\langle Q^2 \rangle = 5.9 \text{ GeV}^2$ is shown in Fig. 5. The underlying contribution due to charm at leading and higher order is also shown. The shape and normalization of the structure functions predicted by PQCD

appears to be consistent with experiment although the detailed results depend on the assumed shape of the photon's gluon distribution. Despite the explicit appearance of the running coupling constant in the leading photon structure function F_2^γ , and the surprisingly good estimate given by the leading order term, model-independent predictions for the normalization of the coefficient of the running coupling constant beyond leading order have proved difficult because of the complications of separating the resolved and direct contributions.²⁶

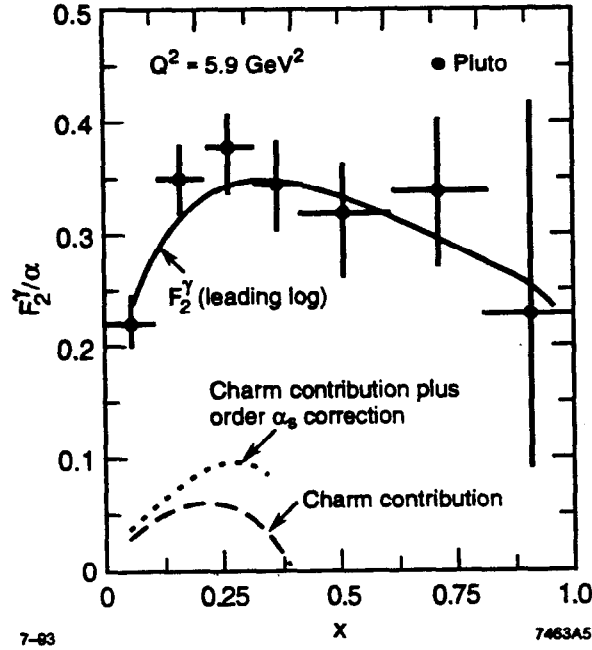


Figure 5. Comparison of perturbative QCD predictions with PLUTO data for the photon structure function at $Q^2 = 5.9 \text{ GeV}^2$. The charm quark contribution from leading and higher order QCD is also shown. From Ref. 25.

The most characteristic behavior of the photon structure function $F_2^\gamma(x, Q^2)$ in QCD is its continuous linear rise of with $\log Q^2$ at fixed x . As emphasized by Peterson, Walsh and Zerwas,²⁷ the fact that this tree graph behavior is preserved to all orders in perturbation theory is due to the balance in QCD between the increase of the phase space for gluon emission in the scattering processes versus the decreasing strength of the gluon coupling due to asymptotic freedom. Although the logarithmic rise of the Born approximation result is preserved, the shape of $h(x)$ is modified by the QCD radiation.

Peterson, Walsh, and Zerwas²⁷ and Miller¹⁸ have considered a *gedanken* modification of QCD such that the running coupling constant freezes to a constant value at large momentum transfer. In this case, as illustrated in Fig. 6, the photon structure function stops rising at high Q^2 due to the increased phase space for gluon radiation.

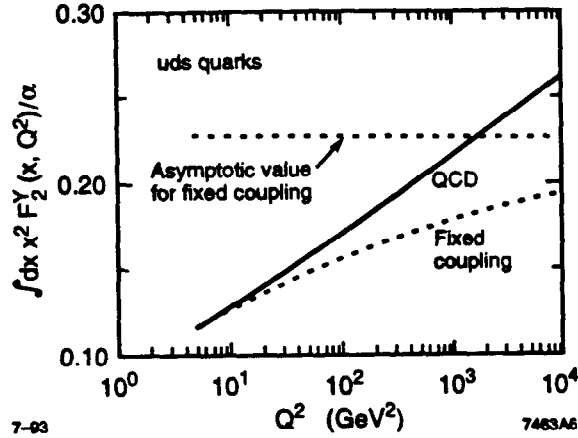


Figure 6. The rise of the photon structure's second moment with $\log Q^2$ as predicted in QCD contrasted to its behavior in a frozen coupling constant theory. From Ref. 27.

Thus probing the QCD photon structure functions at the high momentum transfers available at the NLC will provide a valuable test of asymptotic freedom. However, to make these results definitive, one will need to extend the QCD predictions to include contributions from γZ couplings²⁸ as well as effects due to Higgs, W 's and supersymmetric particles. Extended predictions allowing for both photon and electron polarization are also needed.

A linear collider can also provide a clear and simple test of QCD in the case where both electrons are tagged at large momentum transfer so that both photons are virtual. The leading contributions to the photon structure functions take on the point-like form characteristic of the direct photon couplings to the quarks.

6.1 Jet Physics at a Photon Linear Collider

The distinction between the direct versus resolved hadron-like contributions to photon interactions becomes especially clear in two-photon jet physics. If both photons couple directly to a pair of quarks, the final state is similar to that of e^+e^- annihilation: two co-planar jets are produced without any source of hadronic spectators emitted along the beam direction. Such events would be extraordinarily rare at an the analogous meson-meson collider.

In the case of once-resolved processes, one photon scatters directly on a constituent quark of the other photon, leaving spectators just in one beam direction. In the case of twice-resolved two-photon processes, jets are produced by any of the various qq , qg and gg QCD 2 to 2 scattering subprocesses. Despite their markedly different origins, the cross sections for these two photon jet production processes are

all scale invariant in leading order^{8,29}; that is, in leading logarithm approximation, they each have the form:

$$\frac{d\sigma}{d^3p/E} (\gamma\gamma \rightarrow \text{Jet} + X) = \frac{\alpha^2}{p_T^4} F(x_T, \theta_{cm}) .$$

The logarithmic fall-off of the subprocess cross section is precisely compensated by the increasing strength of the resolved photon structure function. The $x_T = 2p^{\text{jet}}/\sqrt{x}$ dependence of $F(x_T, \theta_{cm})$ has a power-law fall-off at large x_T : $\sim (1 - x_T)^N$ where the index N can be computed at $x \sim 1$ simply by counting the number of beam spectators.⁸

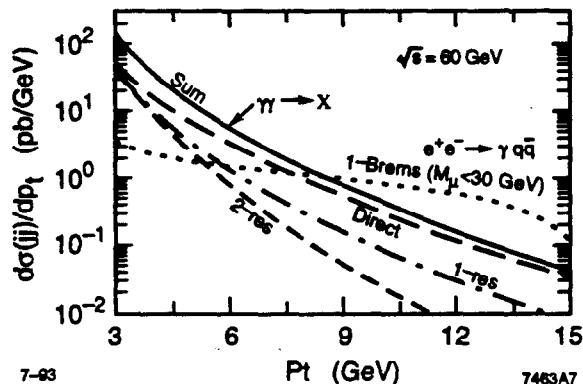


Figure 7. QCD contributions to jet transverse momentum cross section in $\gamma\gamma$ collisions. The resolved contributions are based on the Drees-Godpole model for the gluon distribution in the photon. From Ref. 30.

An illustration of the various contributions to the jet transverse momentum distribution from direct, single and twice resolved contributions as calculated by Drees and Godpole is shown in Fig. 7.³⁰ The dotted curve shows the background from e^+e^- annihilation events with single hard photon radiation from the initial state. A recent comparison of these predictions for single jet and two jet processes with TRISTAN data³¹ obtained from thrust and other jet variable analyses appear to confirm the presence of both direct and resolved contributions, although there are uncertainties from higher order corrections to the jet rate normalization and the assumed form of the photon's gluon distribution. The largest uncertainty in these results is due to the unknown form of the gluon distribution within the resolved photon.^{30,32}

7. Contribution from Mini-Jets to the $\gamma\gamma$ Cross Section

One of the uncertainties concerning QCD predictions for photon-photon collisions is the size of the total inelastic cross section which can be attributed to from mini-jets, i.e., jets of p_T beyond a cutoff of order of a few GeV. Early work by Drees and Godpole³⁰ had suggested that the production rate for mini-jets could rise so fast with energy that mini-jets would provide a significant and troublesome minimum bias background to the study of e^+e^- events at an NLC. However, recent analyses by Forshaw and Storrow³³ and by Chen, Barklow, and Peskin³⁴ have now shown that the rise of the mini-jet rate is moderate into the TeV linear collider regime, and that the resulting backgrounds to physics signals are in fact minimal.

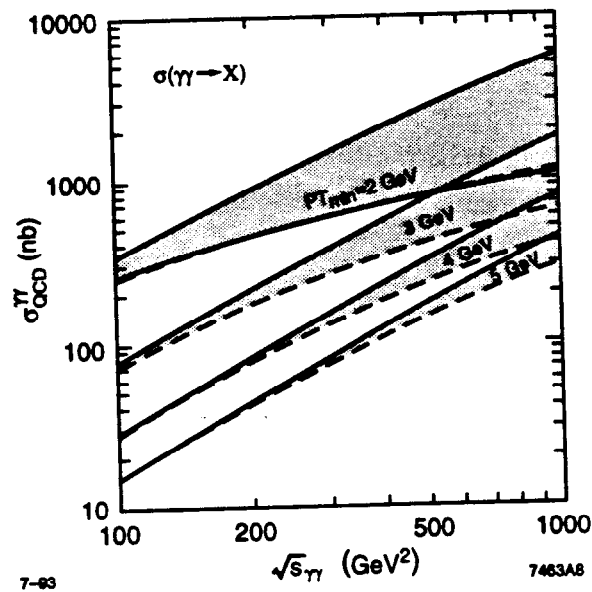


Figure 8. The effect of multiple scattering on the mini-jet contribution to the $\gamma\gamma$ total cross section. The jet contributions are shown for various p_T minimum cut-offs, with (solid line) and without (dashed line) the effect of eikonalization. From Ref. 33.

The new analyses^{34,33} are based on a two-component form for total inelastic cross sections: an energy-independent term σ_0 , plus a rising PQCD contribution obtained by integrating $2 \rightarrow 2$ QCD processes from $p_{t\min} = 3.2$ GeV to the kinematic limit. This parameterization is consistent with the measured rate of mini-jets measured by UA1, the energy dependence of the $p\bar{p}$ cross section, as well as $\sigma_{\gamma p}(s)$ determined by the ZEUS collaboration at HERA. The cross section for mini-jets must be unitarized so that the integral of the cross section $d\sigma/dy$ is normalized to inelastic cross section times the average multiplicity of mini-jets $\langle n \rangle$. As shown in Fig. 8,³³ the eikonalization of the subprocess cross section leads to a significant reduction in the predicted

value and rise with energy of the $\gamma\gamma$ inelastic cross section. The net result for the number of jets with $p_T > 5 \text{ GeV}$ produced per crossing at an NLC is only of order 5 to 8×10^{-2} for typical linear collider designs.

The physics of unitarization has been analyzed from a different perspective by Ginzburg, Ivanov and Serbo.³⁵ In the regime $s_{\gamma\gamma} \gg p_T^2 > \mu^2$, where μ is the confinement scale of QCD, one can apply perturbative QCD to compute the set of gluon exchange chains representing the QCD Pomeron, as in Lipatov's well-known work. It is also possible to compute the double diffractive contribution where two gluon chains to recombine leaving a rapidity gap between the di-jets. Ginzburg *et al.* argue that eikonalization must be taken into account when the rates for these two processes become equal. With this assumption, they find that eikonal corrections must be applied to the perturbative QCD factorized predictions for the jet production cross section at $\sqrt{s_{\gamma\gamma}} = 500 \text{ GeV}$ even at jet transverse momentum as large as $p_T = 26 \text{ GeV}$.

8. The Photon-Hadron Coherence Length

At very high energies the hadronic component of a photon state resembles a coherent sum of vector mesons. The coherence time, as discussed by Ioffe³⁶ and by Yennie *et al.*,³⁷ is $\Delta\tau = \frac{1}{\Delta E} = \frac{2P_\gamma^+}{Q^2 + \mathcal{M}^2}$ for intermediate vector states of mass \mathcal{M} . Thus in high energies photon-nucleus reactions, a real or virtual photon will generally convert to a hadronic system well before interacting in the target, and the energy and nuclear size dependence of the photon-induced cross sections will resemble that of meson-induced reactions. In fact, as shown in Ref. 38, the coherence time of a virtual photon depends on whether its polarization is longitudinal or transverse: $\tau_L = \tau_T/\sqrt{3}$. Thus shadowing of the nuclear photoabsorption cross section will be delayed to higher energies in the case of longitudinal current-nuclear interactions.

The long coherence length between photons and the intermediate vector states at high energies and the resulting photon-hadron duality can be used as a general guide to the hadronic interactions of photons at low transverse momentum. In particular the long coherence length implies pomeron factorization of photon-induced cross sections¹⁴: $\sigma_{\gamma\gamma} = \frac{\sigma_{\gamma p}^2}{\sigma_{pp}}$ Thus one should be able to track the slow increase of the total inelastic photon-photon cross section with that of the γp and pp cross section.

9. Heavy Quark Pair Production in $\gamma\gamma$ Collisions

The leading contributions to heavy quark production in $\gamma\gamma$ collisions are illus-

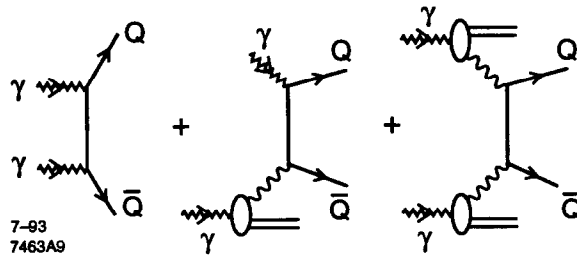


Figure 9. Direct and resolved contributions to heavy quark production in $\gamma\gamma$ collisions.

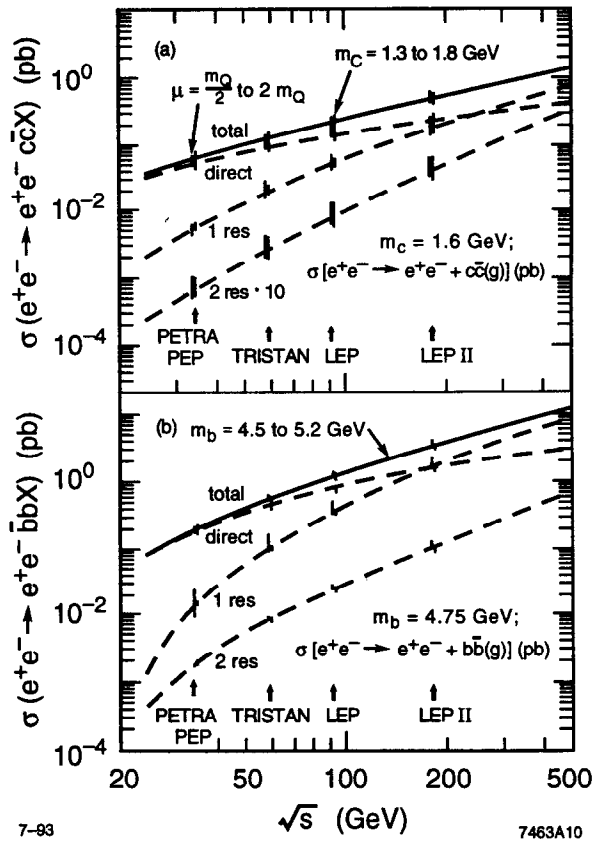


Figure 10. QCD leading and next-to-leading order contributions to the inclusive charm production cross section. The resolved contributions are based on the Drees-Godpole model for the gluon distribution in the photon. From Ref. 40.

trated in Fig. 9. The resolved contributions depend in detail on the assumed form of the photon's gluon distribution.

The cross section for direct heavy quark production $\sigma \sim \pi\alpha^2/m_Q^2$ is of order 130 nb and 1300 pb for $c\bar{c}$ and $b\bar{b}$ production, respectively. The top pair cross section $\sigma_{t\bar{t}}$ is of order of $\frac{1}{2}\sigma_{e^+e^- \rightarrow \mu^+\mu^-}$ at the corresponding energy.^{30,39} Figure 10 shows the prediction of Drees, Kramer, Zunft and Zerwas⁴⁰ for the inclusive charm production cross sections in $e^+e^- \rightarrow e^+e^-q\bar{q}X$ using the equivalent photon approximation. The vertical bars on the left represent the estimated uncertainty due to the scale dependence of the lowest order of predictions. The bar on the right shows the dependence on the quark mass. TPC $\gamma\gamma$ and TRISTAN data for $\sigma(e^+e^- \rightarrow D^{*\pm}X)$ are compared with the QCD prediction of Drees *et al.* in Fig. 11.

Figure 12 a shows the cross section predicted by Kühn, Mirkes and Steegborn⁴¹ for $t\bar{t}$ production including higher order QCD corrections. The predicted rate is given for $m_t = 150$ GeV as a function of the center mass energy of the e^+e^- collider, where a convolution with the computed photon energy spectrum of the back-scattered laser beam is assumed. Once the top mass becomes greater than 120 GeV, its decay width due to weak decays $\Gamma = 2\Gamma(t \rightarrow bW)$ becomes so large that true bound states $t\bar{t}$ cannot form; nevertheless there can be significant threshold effects.^{42,43,44} As shown in Fig. 12b, if $m_t < 200$ GeV and the experiment resolution in $\mathcal{M}_{t\bar{t}}$ is sufficient, then it may be possible to resolve the predicted structure of the $\gamma\gamma \rightarrow t\bar{t}$ cross section near the top threshold. Detailed predictions for this threshold dependence as a function of the top quark mass have been given by Bigi, Gabbiani, and Khoze.⁴³ The combination of $\gamma\gamma$ ($C = +$) and e^+e^- ($C = -$) measurements of the $t\bar{t}$ threshold spectrum could provide a very precise value for the top quark mass.

10. W Pair Production in a $\gamma\gamma$ Collider

One of the most important applications of two photon physics is the direct production of W pairs. By using polarized back-scattered laser beams, one can in principle study $\gamma\gamma \rightarrow W^+W^-$ production as a function of initial photon helicities as well as resolve the W helicities through their decays. The study of $\gamma\gamma \rightarrow W^+W^-$ is complementary to the corresponding $e^+e^- \rightarrow W^+W^-$ channel, but it also can check for the presence of anomalous four-point $\gamma\gamma \rightarrow WW$ interactions not already constrained by electromagnetic gauge invariance, such as the effects due to W^* exchange.

The main focus of the pair production measurements are the values of the W magnetic moment $\mu_W = \frac{e}{2m_W}(1-\kappa-\lambda)$ and quadrupole moment $Q_W = -\frac{e}{M_W^2}(\kappa-\lambda)$. The Standard Model predicts $\kappa = 1$ and $\lambda = 0$, up to radiative corrections analogous to the Schwinger corrections to the electron anomalous moment. The anomalous

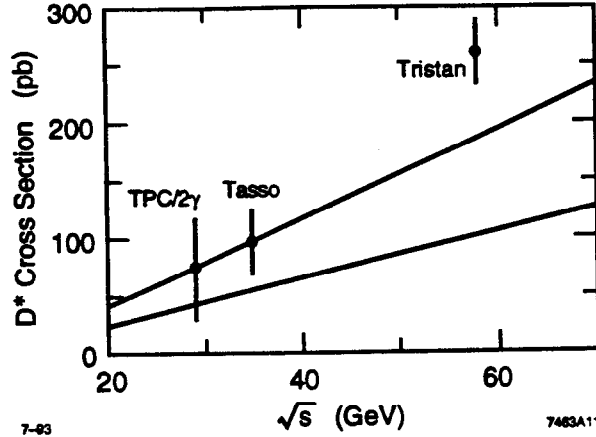


Figure 11. TPC $\gamma\gamma$, TASSO, and TRISTAN data for $\sigma(e^+e^- \rightarrow e^+e^-D^{*\pm}X)$ compared with the QCD prediction of Drees *et al.* From Ref. 40. The dashed lines show the once-resolved contributions. The upper line is $\mu = m_c = 1.3$ GeV. The lower line is $\mu = 2m_c$, $m_c = 1.8$ GeV.

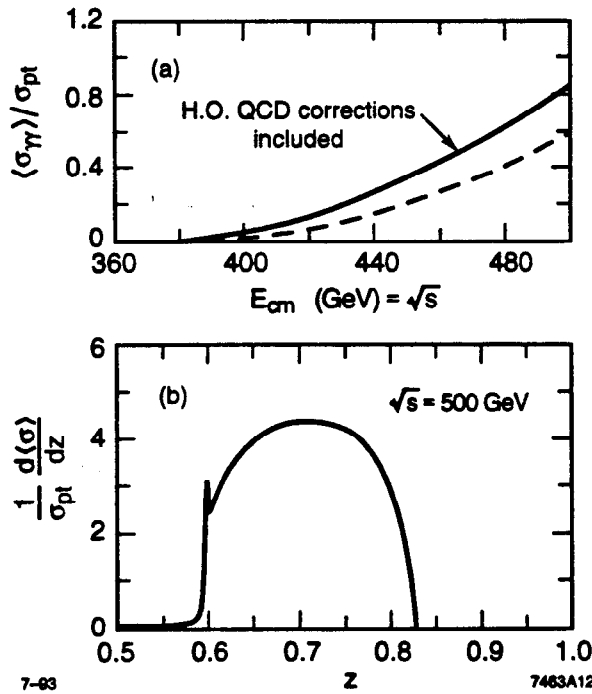


Figure 12. (a) Effective cross section $\langle\sigma(\gamma\gamma \rightarrow t\bar{t})\rangle/\sigma(e^+e^-)_{pt}$ with (solid) and without (dashed) QCD corrections for $m_t = 150$ GeV. The convolution with a back-scattered laser spectrum ($\omega = 1.26$ eV) is included. (b) The effective differential cross section $d\langle\sigma(\gamma\gamma \rightarrow t\bar{t})\rangle/dz/\sigma(e^+e^-)_{pt}$ and the resonance signal predicted at $\sqrt{s_{e^+e^-}} = 500$ GeV. Here $z = \mathcal{M}_{t\bar{t}}/\sqrt{s_{e^+e^-}}$. From Ref. 41.

moments are thus defined as $\mu_A = \mu_W - \frac{e}{M_W}$ and $Q_A = Q_W + \frac{e}{M_W^2}$.

The fact that μ_A and Q_A are close to zero is actually a general property of any spin-one system if its size is small compared to its Compton scale. For example, consider the Drell-Hearn-Gerasimov sum rule⁴⁵ for the W magnetic moment: $\mu_A^2 = (\mu - \frac{e}{M})^2 = \frac{1}{\pi} \int_{\nu_{th}}^{\infty} \frac{d\nu}{\nu} [\sigma_P(\nu) - \sigma_A(\nu)]$. Here $\sigma_{P(A)}$ is the total photoabsorption cross section for photons on a W with (anti-) parallel helicities. As the radius of the W becomes small, or its threshold energy for inelastic excitation becomes large, the DHG integral and hence μ_A^2 vanishes. Hiller and I have recently shown⁴⁶ that this argument can be generalized to the spin-one anomalous quadrupole moment as well, by considering one of the unsubtracted dispersion relations for near-forward γ spin-one Compton scattering⁴⁷:

$$\mu_A^2 + \frac{2t}{M_W^2} \left(\mu_A + \frac{M_2}{W} Q_A \right)^2 = \frac{1}{4\pi} \int_{\nu_{th}}^{\infty} \frac{d\nu^2}{(\nu - t/4)^3} \text{Im}(f_P(s, t) - f_A(s, t)).$$

Here $\nu = (s - u)/4$. One again sees that in the point-like or high threshold energy limit, both $\mu_A \rightarrow 0$, and $Q_A \rightarrow 0$. This result applies to any spin-one system, even to the deuteron or the ρ . The essential assumption is the existence of the unsubtracted dispersion relations; i.e., that the anomalous moments are in principle computable quantities.

In the case of the W , the finite size correction is expected to be order m^2/Λ^2 , since the underlying composite theory should be chiral to keep the W mass finite as the composite scale, Λ becomes large.⁴⁸ Thus the fact that a spin-one system has nearly the canonical values for its moments signals that it has a small internal sizes; however, it does not necessarily imply that it is a gauge field.

Yehudai⁴⁹ has made extensive studies of the effect of anomalous moments on different helicity amplitude contributing to $\gamma\gamma \rightarrow W^+W^-$ cross section. Figure 13 shows the differential cross section for the process $\gamma\gamma \rightarrow W^+W^-$ in units of $\sigma_{e^+e^- \rightarrow \mu^+\mu^-}$ as a function of center mass angle for $\lambda = 0, 0.1$ and $\kappa = 1, 0.1$. The empirical sensitivity to anomalous couplings from $\gamma\gamma$ reactions is comparable and complimentary to that of $e^+e^- \rightarrow W^+W^-$.

11. Vector Boson Pair Production in Photon-Photon Collisions

As emphasized by Jikia,⁵⁰ pairs of neutral gauge bosons of the Standard model

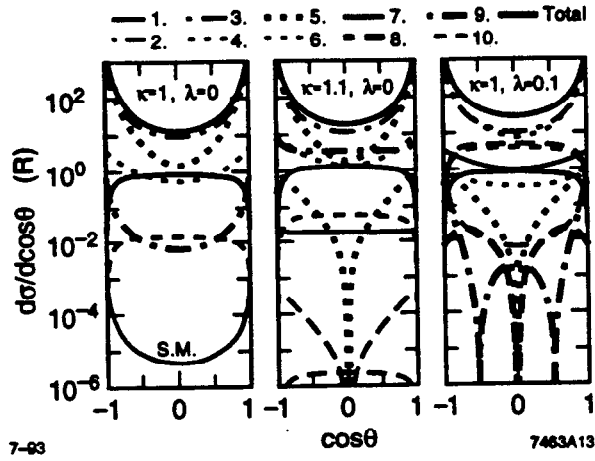


Figure 13. Differential cross sections for producing a W pair of a specific helicity combination at $\sqrt{s_{\gamma\gamma}} = 500$ GeV as a function of $\cos\theta$. The curves are:

- 1: $(++++)+(-)$, 2: $(++++)+(++++)+(-+)+(-+)$,
- 3: $(++-)+(-++)$, 4: $(-++)+(-++)+(+-)+(-+-)$,
- 5: $(+-)+(-++)+(-++)+(+-)$,
- 6: $(+-)+(-+0)+(-+0)+(-++0)+(-++0)+(-+0)+(-+0)+(-+0)+(-+0)$,
- 7: $(+00)+(-+00)$, 8: $(++0+)+(-0)+(+++0)+(-0)$,
- 9: $(++00)+(-00)$, 10: $(++0-)+(++-0)+(-0+)+(-0)$.

The notation indicates $(\lambda_1\lambda_2\lambda_3\lambda_4)$, where $\lambda_1, \lambda_2, \lambda_3$ and λ_4 are the helicities of the two photons and the W^+ and the W^- respectively. From Ref. 49.

can be produced in $\gamma\gamma$ reactions through one loop amplitudes in the Standard Model at a rate which should be accessible to the NLC. For example, the Standard Model one-loop contributions for the reaction $\gamma\gamma \rightarrow Z^0 Z^0$ is shown in Figure 14. These high energy physics “petroglyphs” are computed by Jikia using the background nonlinear gauge in order to avoid four-point couplings between the ghost fields and the W fields. The ghost fields include Faddeev-Popov ghost fields as well as scalar W auxiliary fields.

A familiar example of this type of quantum mechanical process is the production of large invariant mass $\gamma\gamma$ final states through light-by-light scattering amplitudes. Leptons, quarks, and W all contribute to the box graphs. The fermion and spin-one exchange contributions to the $\gamma\gamma \rightarrow \gamma\gamma$ scattering amplitude have the characteristic behavior $\mathcal{M} \sim s^0 f(t)$ and $\mathcal{M} \sim i s f(t)$ respectively. The latter is the dominant contribution at high energies, so one can use the optical theorem to relate the forward imaginary part of the scattering amplitude to the total $\gamma\gamma \rightarrow W^+W^-$ cross section.⁵⁰ The resulting cross section $\sigma(\gamma\gamma \rightarrow \gamma\gamma)$ is of order 20 fb at $\sqrt{s_{\gamma\gamma}}$, corresponding to 200 events/year at an NLC with luminosity 10 fb^{-1} .

Figure 15 shows the effective cross section for $\gamma\gamma \rightarrow Z^0\gamma$ at an NLC assuming

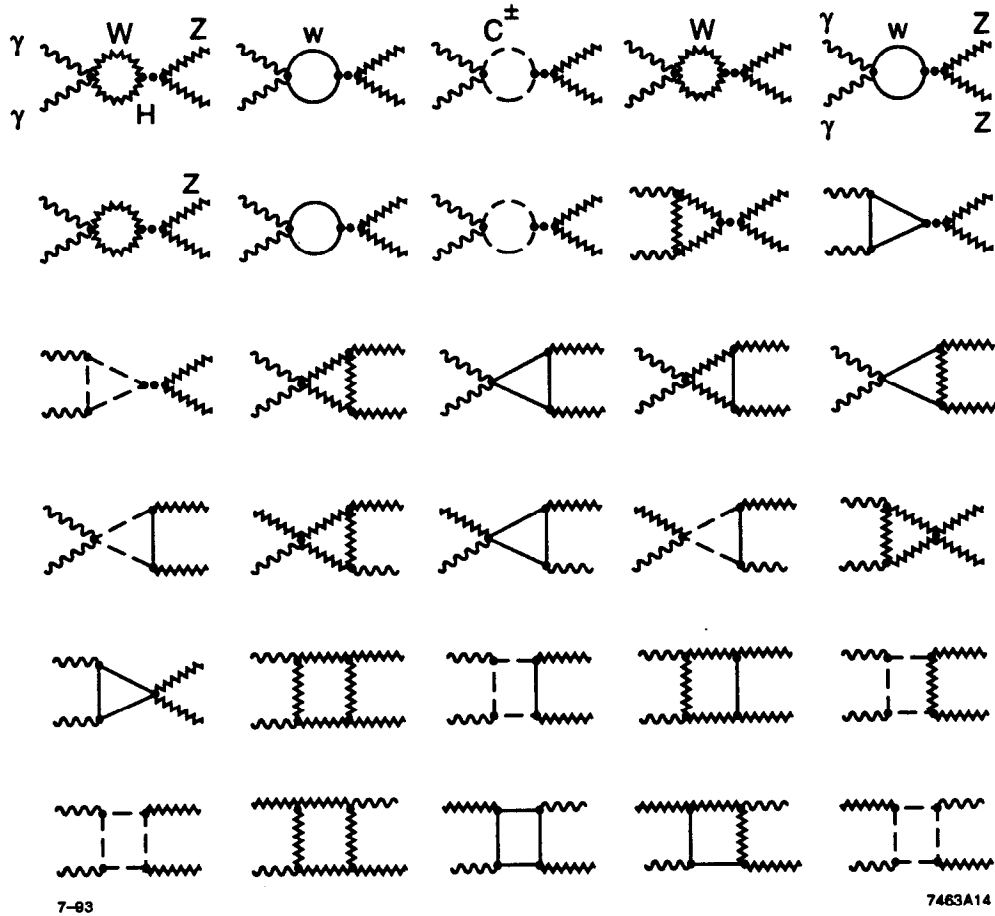


Figure 14. Standard Model one-loop contributions to the reaction $\gamma\gamma \rightarrow ZZ$ including ghost c^\pm and scalar w contributions in the background nonlinear gauge. From Ref. 50.

the back-scattered laser spectrum.⁵⁰ The rate for transversely polarized Z dominates strongly over longitudinal Z , reflecting the tendency of the electroweak couplings to conserve helicity. The cross section for $\gamma\gamma \rightarrow Z_T\gamma$ at $\sqrt{s_{e^+e^-}} = 500$ GeV is estimated by Jikia to be 32 fb, corresponding to 320 NLC events/year. As we discuss below, the channel $\gamma\gamma \rightarrow Z_T Z_T$ provides a serious background to Higgs production in $\gamma\gamma$ collisions.

12. Resonance Production at a Photon-Photon Collider

A unique advantage of a photon-photon collider is its potential to produce and determine the properties of fundamental $C = +$ resonances such as the Higgs boson, as illustrated in Fig. 1.^{51,14} The resonance condition is $(q_1 + q_2)^2 = 4\omega_1\omega_2 = M_H^2$. The

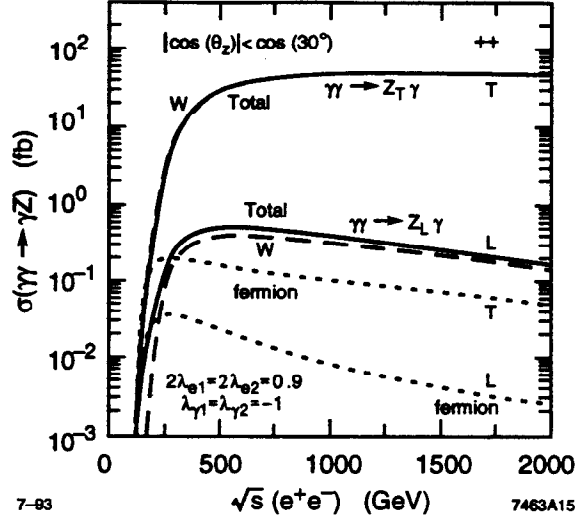


Figure 15. The effective cross section for $\gamma\gamma \rightarrow Z^0\gamma$ at an NLC taking into account the back-scattered laser spectrum. The fermion and W loop contributions are shown for the production of a transversely (T) and longitudinally (L) polarized Z^0 . The incident photons are taken to have positive helicity. From Ref. 50.

initial state resolution is unavoidably broadened when one folds in the back-scattered laser energy spectrum. Explicit calculations are given in Refs. 52, 53, and 54. One can also use the transverse polarization of the colliding photons to distinguish the parity of the resonance: the coupling for a scalar resonance is $\epsilon_1 \cdot \epsilon_2$ versus $\epsilon_1 \times k_1 \cdot \epsilon_2$ for the pseudoscalar. More generally, one can use polarized photon-photon scattering to study CP violation in the fundamental Higgs to two-photon couplings.⁵⁵ In the case of electron-photon collisions, one can use the transverse momentum fall-off of the recoil electron in $e\gamma \rightarrow e'H^0$ to measure the fall-off of the $\gamma \rightarrow$ Higgs transition form factor and thus check the mass scale of the internal massive quark and W loops coupling to the Higgs.⁵⁶

The present-day analog of $\gamma\gamma \rightarrow$ Higgs production is the production of narrow charmonium states. For example, the TPC $\gamma\gamma$ collaboration at PEP⁵⁷ has reported the observation of 6 η_c events, which gives $\Gamma_{\gamma\gamma}(\eta_c) = 6.4^{+5.0}_{-3.4} \text{ KeV}$. Higher luminosity facilities such as CESR or a B-factory should allow extensive measurements of $\gamma\gamma$ physics at the charm threshold.

If the Higgs has a mass less than 140 GeV, its dominant decay channel is $H \rightarrow b\bar{b}$. The signal for $\gamma\gamma \rightarrow H \rightarrow b\bar{b}$ for Higgs masses in this region must then compete with heavy quark backgrounds such as those shown in Fig. 16.⁵⁸ The partial cross section $\sigma(\gamma\gamma \rightarrow H \rightarrow b\bar{b})$ and backgrounds are evaluated for a range of Higgs mass, assuming the resolution in the mass of the $b\bar{b}$ system is ± 10 GeV, the b -quark angular acceptance is $|\cos\theta| < 0.85$, and the b rapidity range is $|y| < 1.5$. Since the

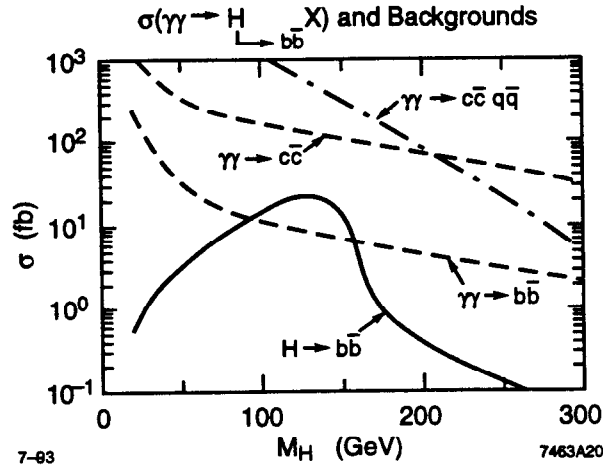


Figure 16. The partial cross section $B(H \rightarrow \bar{b}b)\sigma(\gamma\gamma \rightarrow H^0)$ compared with heavy quark pair production backgrounds. The experimental resolution in the $\bar{b}b$ mass is assumed to be 10 GeV. From Ref. 58.

signal is much less than the heavy quark cross sections, it will be essential to have efficient b tagging and excellent mass resolution.

When the mass of the Higgs is greater than twice the Z mass, its major decay channel will be $H \rightarrow Z_L Z_L$. However, as Jikia⁵⁰ has emphasized, the continuum background from $\gamma\gamma \rightarrow Z_T Z_T$ is very large. An estimate of the magnitude of the background cross section, $\sigma(\gamma\gamma \rightarrow Z_T) \sim Z_T \sim 250$ fb can be obtained simply by scaling the $\gamma\gamma \rightarrow \gamma\gamma$ rate by the coupling $g_{WWZ}^4/e^4 \sim 11$ since the amplitude is dominated by the W loop. However, it appears possible to discern the Higgs signal in $\gamma\gamma$ collisions if the Higgs mass is 300 GeV or less, and one has excellent resolution in the ZZ invariant mass. (See Fig. 17.). One also has to suppress the very large backgrounds from $\gamma\gamma \rightarrow W^+W^-$. For example, Jikia⁵⁰ considers the case $M_H = 300$ GeV, at $\sqrt{s_{e^+e^-}} = 400$ GeV. After folding in the spectrum of the back-scattered laser beams, he estimates number of events in the range $290 < M_{ZZ} < 310$ GeV in one NLC year is 100; 70 from $H \rightarrow Z_L Z_L$, and 30 from the background.

Jikia⁵⁹ and Bowser-Chao *et al.*⁶⁰ have also shown that the rate of $\gamma\gamma$ to 2 Higgs is not negligible compared to the single Higgs rate. The cross section for $\sigma(\gamma\gamma \rightarrow HH)$ is shown in Fig. 18 as a function of Higgs mass. Again one sees that the W loop contributions generally dominate for the expected range of top quark masses.

13. Single Top Quark Production

A single top quark can be produced in electron-photon collisions at an NLC

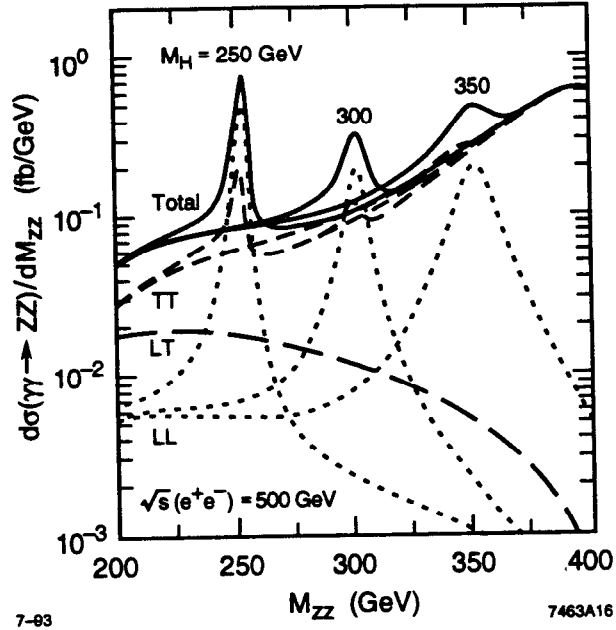


Figure 17. Comparison of the Higgs signal in $\gamma\gamma$ collisions for $M_H = 250, 300,$ and 350 GeV at $\sqrt{s_{e^+e^-}} = 500$ GeV with the background from $\gamma\gamma \rightarrow ZZ$. The angular cut $|\cos(\Theta)| < \cos 30^\circ$ was imposed. From Ref. 50.

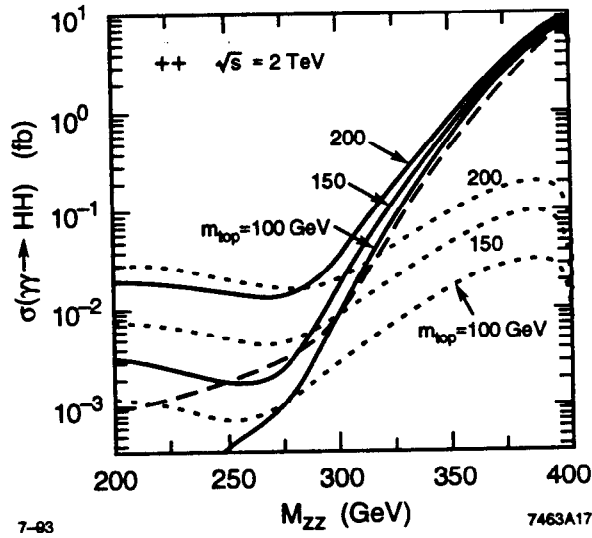


Figure 18. The total $\gamma\gamma \rightarrow HH$ Higgs pair production cross section at $\sqrt{s_{\gamma\gamma}} = 2$ TeV for equal photon helicities $\lambda_1 = \lambda_2 = 1$ as a function of the Higgs mass. The solid line is the total cross section, the dashed line is the W boson contribution, and the dotted line is the top quark contribution. The results are shown for $m_t = 100, 150$ and 200 GeV. From Ref. 50.

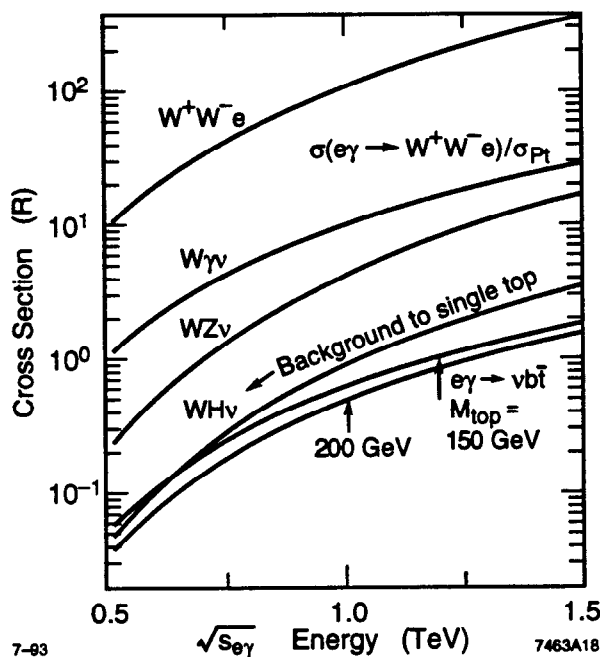


Figure 19. The single top production cross section and its competing backgrounds in high energy electron-photon collisions. From Ref. 53.

through the process $e^- \gamma \rightarrow W^- t \bar{\nu}$.^{61,53} This process can be identified through the $t \rightarrow W^+ b$ decay with $W \rightarrow \ell \bar{\nu}$. The rate is thus sensitive to the V_{tb} matrix element and possible fourth generation quarks and anomalous couplings. An interesting background is the virtual W process $e \gamma \rightarrow W^* - \nu \rightarrow W^- H \nu$, where the Higgs boson decays to $b \bar{b}$ and $W^- \rightarrow \ell \bar{\nu}$. The rates for the signal and background processes as a function of $\sqrt{s_{e^+e^-}}$ computed by Cheung⁵³ and Yehudai⁴⁹ are shown in Fig. 19.

14. Higgs Plus Top Quark Pair Production

The tree process $\gamma \gamma \rightarrow t \bar{t} + H$ can provide a direct measure of coupling of the Higgs boson to heavy quarks. The cross section has been estimated by Boos⁵⁴ and Cheung⁵³ to be of order 1 to 5 fb. Cheung⁵³ has also computed the radiative corrections to $\gamma \gamma t \bar{t}$ from final state Higgs exchange interactions. The correction is of $\mathcal{O}(2 - 4\%)$ for typical values of the Higgs boson mass and top quark mass.

15. Single and Double Diffraction in Photon-Photon Collisions

The high energies of a $\gamma\gamma$ collider will make the study of double diffractive $\gamma\gamma \rightarrow V^0 V^0$ and semi-inclusive single diffractive processes $\gamma\gamma \rightarrow V^0 X$ in the Regge regime $s \gg |t|$ interesting. (See Fig. 20.) Here $V^0 = \rho, \omega, \phi, J/\psi, \dots$. If $|t|$ is taken larger than the QCD confinement scale, then one has the potential for a detailed study of fundamental Pomeron processes and its gluonic composition.⁶² As in the case of large angle exclusive $\gamma\gamma$ processes, the scattering amplitude is computed by convoluting the hard scattering PQCD amplitude for $\gamma\gamma \rightarrow q\bar{q}q\bar{q}$ with the vector meson distribution amplitudes. As shown by Chernyak and Zhitnitsky,⁶³ the two gluon exchange contribution dominates in the Regge regime, giving a characteristic exclusive process scaling law of order $\frac{d\sigma}{dt} (\gamma\gamma \rightarrow V^0 V^0) \sim \alpha_s^4(t)/t^6$. Recently, Ginzburg *et al.*¹¹ have shown that the corresponding $\gamma\gamma \rightarrow$ pseudoscalar and tensor meson channels can be used to isolate the Odderon exchange contribution, that is contributions related at a fundamental level to three gluon exchange.

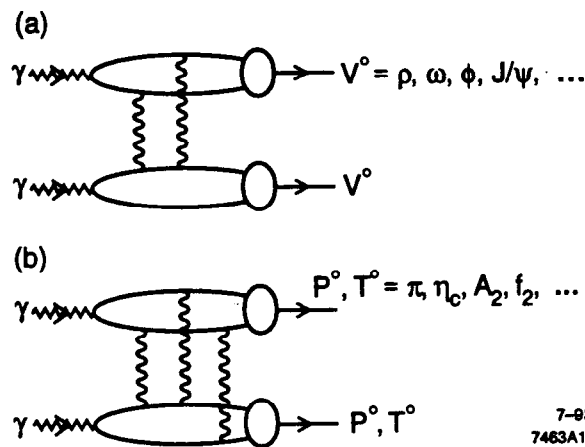


Figure 20. Perturbative QCD contributions to large momentum transfer exclusive double diffractive $\gamma\gamma$ processes. The two-gluon exchange pomeron contributions to vector meson pair production and three-gluon exchange odderon contributions to neutral pseudoscalar and tensor meson pair production are illustrated.

16. Conclusions

Photon-photon collisions at a linear e^+e^- collider in the TeV range will provide an extraordinary window for testing electroweak and QCD phenomena as well as proposed extensions of the Standard Model, such as supersymmetry,⁶⁴ technicolor, and other composite models. Two-photon physics is unique in that virtually all charged particles and their bound states and resonances with positive C can be

produced; in addition one can access pairs of fundamental neutral particles through one-loop corrections. It will be essential to have the capability of back-scattered laser beams at the NLC, since it is expected that the resulting luminosity and effective energy of photon-photon and photon-electron collisions will be comparable to that of the primary e^+e^- collisions. Such a facility, together with polarized electron beams, will also allow the study of the physics of highly-polarized photon-photon and electron-photon collisions. There is also a wide range of physics topics which could be addressed in polarized electron-electron collisions, if such a capability were available at the NLC.⁶⁵

Two-photon physics is an extensive phenomenological field, having elements in common with both e^+e^- and hadron-hadron collisions. However, the combination of direct photon and resolved processes gives two photon physics an extra dimension in probing new phenomena. For example, since each photon can be resolved into a W^+W^- pair, high energy photon-photon collisions can provide a remarkably background-free laboratory for studying WW collisions and annihilation. Thus a photon-photon collider can also become the equivalent a WW collider to study whether the interactions of longitudinally polarized W 's are controlled by Higgs annihilation and exchange or a new type of strong interaction.

It is clear that gg collisions are an integral part of the NLC physics program. It was possible to highlight only a small part of the possible new $\gamma\gamma$ physics topics here. At present energies, studies of $\gamma\gamma$ collisions at CESR, PETRA, PEP, TRISTAN, and LEP have led to a number of important tests of perturbative and non-perturbative QCD in exclusive and inclusive reactions, heavy quark phenomena, and resonance formation. Reviews of the results of these experiments and the underlying theory of $\gamma\gamma$ collisions are given in Refs. 1, 2, 4, 5 and in the proceedings of the International Workshops on Photon-Photon collisions.

Acknowledgments

I am grateful to David Borden, Michael Boulware, George Jikia, Ilya Ginzburg, and Peter Zerwas for helpful conversations.

REFERENCES

1. H. Kolanoski and P. Zerwas, DESY 87-185 (1987), published in "High Energy Electron-Positron Physics," eds. A. Ali and P. Söding, World Scientific, Singapore.
2. J. H. Field, preprint L.P.N.H.E. 84-04 (1984).
3. Ch. Berger and W. Wagner, *Phys. Rep.* **136** (1987) 1.
4. H. Kolanoski, Two-Photon Physics at e^+e^- Storage Rings, Springer Verlag, (1984)
5. S. J. Brodsky, in the proceedings of the IXth International Workshop on Photon-Photon Collisions, Shresh, Israel (1988).
6. D. L. Borden, D. A. Bauer, D. O. Caldwell, SLAC-PUB-5715 (1992).
7. S. J. Brodsky, G. Jikia, and F. Schlumpf, to be published.
8. The descriptive terms, direct and resolved, were introduced by Drees and Godpole.³⁰ See also S. J. Brodsky, T. DeGrand, J. Gunion, and J. Weis, *Phys. Rev. Lett.* **41** (1978) 672; *Phys. Rev.* **19**, (1979) 1418.
9. For a review of two-photon exclusive processes, see S. J. Brodsky, proceedings of the IXth International Workshop on Photon-Photon Collisions, D. Caldwell and H. Paar, eds. (World Scientific, 1992.)
10. T. Hyer, *Phys. Rev.* **D47** (1993) 3875.
11. See I. F. Ginzburg, these proceedings, and the proceedings of the IXth International Workshop on Photon-Photon Collisions, D. Caldwell and H. Paar, eds. (World Scientific, 1992.)
12. G. P. Lepage and S. J. Brodsky, *Phys. Rev.* **D22** (1980) 2157. S. J. Brodsky and G. P. Lepage, *Phys. Rev.* **D24** (1981) 1808; **D24** (1981) 2848.
13. I. Ginzburg, G. Kotkin, V. Serbo, and V. Telnov, *JETP Lett.* **34** (1982) 491. For further references and reviews see the contributions of V. Telnov, V. Balakin and I. F. Ginzburg, and D. Borden, these proceedings, and the reports of V. Telnov and J. Spencer in the proceedings of the IXth International Workshop on Photon-Photon Collisions, D. Caldwell and H. Paar, eds. (World Scientific, 1992.)
14. S. J. Brodsky, T. Kinoshita, and H. Terazawa, *Phys. Rev. Lett.* **25** (1970) 972; *Phys. Rev.* **D4** (1971) 1532.
15. R. Blankenbecler and S. D. Drell, *Phys. Rev. Lett.* **61** (1988) 2324; *Phys. Rev.* **D37** (1988) 3308; *Phys. Rev.* **D36** (1987) 277.
16. M. Jacob and T. T. Wu, in the proceedings of the Lepton/Photon Symp. (1991); *Phys. Lett.* **B216** (1989) 442; *Phys. Lett.* **197B** (1987) 253.

17. The spectrum of beamstrahlung photons depends on the machine design; see T. Barklow, P. Chen, and W. Kozanecki, SLAC-PUB 5718 (1992) and DESY 92-123 B (1992).
18. D. Miller, these proceedings.
19. A. Djouadi, M. Spira, and P. M. Zerwas, DESY 92-170. K. Melnikov and O. Yakovlev, Novosibirsk BUDKERINP preprint 93-4 (1993).
20. Higgs production in electron-photon collisions is discussed K. Hagiwara I. Watanabe, and P. M. Zerwas, *Phys. Lett.* **B278** (1992) 187. See also M. Baillargeon and F. Boudjema, ENSLAPP-A-400-92, Aug 1992.
21. S. J. Brodsky, T. Kinoshita, and H. Terazawa, *Phys. Rev. Lett.* **27** (1971) 280.
22. T. F. Walsh, *Phys. Lett.* **36B** (1971) 121. T. F. Walsh and P. M. Zerwas, *Phys. Lett.* **44B** (1975) 195.
23. R. J. DeWitt, L. M. Jones, J. D. Sullivan, D. E. Willen, H. W. Wyld, Jr., *Phys. Rev.* **D19** (1979) 2046.
24. E. Witten, *Nucl. Phys.* **B120** (1977) 189.
25. E. Laenen, S. Riemersa, J. Smith, and W. L. van Neerven, Stony Brook preprint ITP-SB-93-1 (1993).
26. For a review and further references, see P. Kessler, in the proceedings of the IXth International Workshop on Photon-Photon Collisions, D. Caldwell and H. Paar, eds. (World Scientific, 1992.)
27. C. Peterson, T. F. Walsh, and P. Zerwas, *Nucl. Phys.* **B229** (1983) 445.
28. See A. Cordier et al, LEP200 Workshop, CERN 87-08 (1987).
29. C. H. Llewellyn Smith, *Phys. Lett.* **B79** (1979) 83.
30. M. Drees and R. M. Godpole, these proceedings, *Nucl. Phys.* **B339** (1990) 355; *Phys. Rev. Lett.* **67** (1992) 1189; and DESY 92-044 (1992). M. Drees , DESY 92-065 (1992).
31. T. Tauchi, *et al.*, these proceedings. H. Hayashii, *et al.*, KEK-Preprint-93-47, (1993).
32. H. Abromowicz, K. Charchula, and A. Levy, *Phys. Lett.* **B269** (1991) 458. A. Levy, proceedings of the IXth International Workshop on Photon-Photon Collisions, D. Caldwell and H. Paar, eds. (World Scientific, 1992.)
33. J. K. Storrow, these proceedings. J. R. Forshaw and J.K. Storrow, proceedings of the IXth International Workshop on Photon-Photon Collisions, D. Caldwell and H. Paar, eds. (World Scientific, 1992.); *Phys. Rev.* **D46** (1992) 4955.
34. P. Chen, these proceedings. P. Chen, T. L. Barklow, M. E. Peskin, SLAC-PUB-5873 (1993).

35. I. Ginzburg, these proceedings
36. B. L. Ioffe, *Phys. Lett.* **30B** (1969) 123; J. Pestieau, P. Roy, and H. Terazawa, *Phys. Rev. Lett.* **25** (1970) 402; A. Suri and D. R. Yennie, *Ann. Phys. (N.Y.)* **72** (1972) 243. See also, L. Stodolsky, in the *Proceedings of the International School of Elementary Particle Physics*, Herceg-Novci, Yugoslavia, (1969). Edited by M. Nikolic. N.Y., Gordon and Breach, 1977.
37. T. H. Bauer, R. D. Spital, and D. R. Yennie, *Rev. Mod. Phys.* **50** (1968) 261.
38. V. Del Duca, S. J. Brodsky, and P. Hoyer, *Phys. Rev.* **D46** (1992) 931.
39. O. J. P. Eboli, M. C. Gonzalez-Garcia, F. Halzen, and S. F. Novaes, *Phys. Rev.* **D47** (1993) 1889 and *Phys. Lett.* **B301** (1993) 115.
40. M. Drees, M. Krämer, J. Zunft, and P. M. Zerwas, DESY 92-169 (1992).
41. J. H. Kühn, E. Mirkes, and J. Steegborn, Karlsruhe preprint TTP92-28 (1992).
42. J. H. Kühn and P. M. Zerwas, *Phys. Rept.* **167** (1988) 321.
43. I. L. Bigi, F. Gabbiani, and V. A. Khoze, SLAC-PUB 5951 (1992).
44. S. J. Brodsky, G. Köpp, and P. M. Zerwas, *Phys. Rev. Lett.* **58** (1987) 443.
45. S. D. Drell and A. C. Hearn, *Phys. Rev. Lett.* **16** (1966) 908; S. B. Gerasimov. *Yad. Fiz* **2** (1965) 598 [*Sov. J. Nucl. Phys.* **2** (1966) 430]; M. Hosoda and K. Yamamoto, *Prog. Theor. Phys.* **36** (1966) 426; see also S. J. Brodsky and J. R. Primack, *Ann. Phys. (N.Y.)* **52** (1960) 315.
46. S. J. Brodsky and J. R. Hiller, *Phys. Rev.* **D46** (1992) 2141.
47. W.-K. Tung, *Phys. Rev.* **176** (1968) 2127.
48. S. J. Brodsky and S. D. Drell, *Phys. Rev.* **D22** (1980) 2236.
49. E. Yehudai, these proceedings, SLAC-383 (1991); *Phys. Rev.* **D44** (1991) 3434; *Phys. Rev.* **D41** (1990) 33.
50. G. Jikia, these proceedings, *Phys. Lett.* **B298** (1993) 224, and Protvino preprints IHEP 93-37 (1993). E. E. Boos and G.V. Jikia *Phys. Lett.* **B275** (1992) 164.
51. F. E. Low, *Phys. Rev.* **120** (1960) 582.
52. D. L. Borden, D. A. Bauer, and D. O. Caldwell, UCSB-HEP 93-01 (1993).
53. K. Cheung, these proceedings, and Northwestern preprint NUHEP-TH-93-3, (1993). See also K. Cheung, *Phys. Rev.* **D47** (1993) 3750.
54. E. Boos, these proceedings, and E. Boos, I. Ginzburg, K. Melnikov, T. Sack, and S. Shichanin, *Z. Phys.* **56** (1992) 487.
55. B. Grzadkowski and J.F. Gunion, *Phys. Lett.* **B294** (1992) 361.
56. Wai-Keung Tang, to be published.

57. H. Aihara *et al.*, *Phys. Rev. Lett.* **60** (1988) 2355.
58. O. J. P. Eboli, M. C. Gonzalez-Garcia, F. Halzen, and D. Zeppenfeld, Wisconsin preprint MAD/PH/743 (1993). For other backgrounds to Higgs production see I. F. Ginzburg and V. G. Serbo, these proceedings.
59. G. Jikia, Protvino preprint, IHEP 92-91.
60. D. Bowser-Chao, K. Cheung, and S. Thomas, Northwestern preprint NUHEP-TH-93-7 (1993).
61. G. V. Jikia, *Nucl. Phys.* **B374** (1992) 83.
62. I. F. Ginzburg, these proceedings, and I. F. Ginzburg and D. Yu. Ivanov, *Nucl. Phys.* **B388** (1992) 376.
63. V. L. Chernyak and I. R. Zhitnitsky, *Phys. Rep.* **112** (1984) 1783. Novosibirsk Inst. Nucl. Phys. Acad. Sci. preprint 82-44 (1982)
64. F. Cuypers, G. van Oldenborgh, R. Rückl, CERN-TH 6742/92 (1992). *Nucl. Phys.* **B383** (1992) 45.
65. See, for example, P. H. Frampton, *Mod. Phys. Lett.* **A7** (1992) 2017, and the contributions of C. Heusch and P. H. Frampton to these proceedings.